This is a preprint of the paper that appeared in:
Proceedings of the 2002 IEEE/RSJ International Conference on Intelligent Robots and Systems, Lausanne, Switzerland,
September 30 - October 4 (2002) 2491-2496.

Actuator Selection and Hardware Realization of a Small and Fast-Moving, Autonomous Humanoid Robot

Dirk Wollherr° Michael Hardt* Martin Buss° Oskar von Stryk*

° *Control Systems Group, Technical University Berlin,* www.rs.tu-berlin.de
* *Simulation and Systems Optimization Group, Technische Universität Darmstadt,*
www.sim.informatik.tu-darmstadt.de

Abstract

This paper discusses the design concept and system development of a small and relatively fast walking, autonomous humanoid robot with 17 degrees-of-freedom (DoF). The selection of motor size and gear ratios is based on numerical optimization of detailed multibody dynamics and optimal control corresponding to fast steps of the robot with an envisioned target speed of more than 0.5 m/s. In this paper the design considerations based on numerical optimal control studies and the mechanical realization of the robot are presented including first investigations on the achievable performance of a decentralized, microcontroller-based control architecture.

1 Introduction

Many research groups and companies are developing biped, humanoid walking machines, see e.g. [1–6]; applications are plentiful, ranging from robot soccer, entertainment [7–9], to home care [10]. This paper presents the design, development strategies and the mechanical realization of a new small size and fast, autonomous humanoid walking machine trying to keep the mechanical construction as simple, cheap, and lightweight as possible. The design concept is kinematically similar to PINO [11] and the Sony dream robot 3DR [7] but uses off-the-shelf, high performance DC motors.

One self-imposed demand for the design is that the robot should consist only of a small number of identical mechatronic modules linked together. Considering cost, the hardware design is based on commercially available components whenever possible. With no small, lightweight, and inexpensive motion control board being commercially available a microcontroller based board integrating a complete control loop has been developed. Reference and measured signals are exchanged with the central PC via the USB bus.

The key focus is to create an autonomous humanoid robot for fast, dynamic walking. Numerical simulation and optimization of full nonlinear dynamic models are used throughout the design and control development process.

The selection of motors and gears is presented in the first step of robot design. It is based on fitting the most appropriate motors and gears to the generated minimal energy trajectories subject to power constraints balancing between system weight and motor power. The optimizations are performed for a walking speed of $> 0.5\,\mathrm{m/s}$. The robot geometry is largely imposed by the RoboCup rules [12]. As the total height of the robot is 70–80 cm, this velocity requires roughly 3–4 steps per second.

For the organization of this paper: Section 2 describes design considerations based on optimal control solutions of robot steps. The practical realization of the robot is discussed in Section 3.

2 Design based on Optimal Control

2.1 Robot Kinematic Structure

A preliminary architecture used for the 70 cm humanoid robot consists of 3-dimensional blocks for the links as shown in Fig. 1 and with dimensions given in Table 1. For the simulations during actuator selection a reduced model, neglecting the navel joint, thus having 16 DoF has been employed. Each robot leg features 6 DoF: 2 DoF in the ankle joint to allow for forward and lateral movement, 1 DoF in the knee joint, and 3 DoF in the hips for a full range of movement. Two DoF are placed in each shoulder to compensate the leg momenta with the swing of the arms and to provide lateral stability. Two different weight classes were initially considered for the robot to be constructed: a heavy 18 kg version and a lightweight model with 12 kg mass. The links are modeled with uniformly distributed mass where the masses are listed in Table 1.

The following calculations have been performed with a footless model in order to select the joint motors and gears by dynamic optimization. The flexible con-

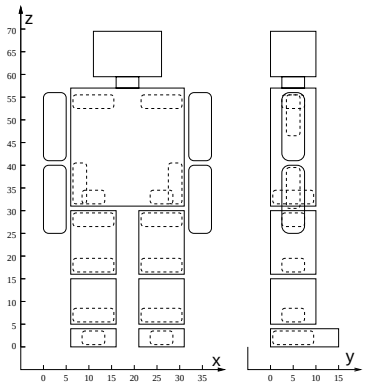

Figure 1: *Preliminary Complete Model*

Table 1: *Link dimensions and masses*

	Torso	Thigh	Shank
d_x [m]	0.1	0.14	0.15
d_y [m]	0.25	0.1	0.1
d_z [m]	0.385	0.1	0.1
12 kg model [kg]	7.355	1.161	1.161
18 kg model [kg]	11.03	1.742	1.742

struction of the links as described in Sec. 3.1 is assumed to have a shock absorption effect thus reducing the peak load to be taken up by the joints.

As one of the design goals is high speed walking, the power of the motors and the gear ratios are now optimized based on these mechanical and geometrical constraints.

2.2 Optimized Walk of a Biped

The biped is optimized over one phase where the movement is constrained to the sagittal plane (vertical plane of forward movement). Each leg instantaneously lifts off from the ground when the other collides with the ground representing the most efficient form of walking without feet. The collision is modeled as perfectly inelastic.

The dynamical model used here is that of rigid, multibody system experiencing contact forces

$$\begin{aligned}\dot{\mathbf{q}} &= k(\mathbf{v})\\ \dot{\mathbf{v}} &= \mathcal{M}(\mathbf{q})^{-1}\Big(\mathbf{S}\mathbf{u} - \mathcal{C}(\mathbf{q},\mathbf{v}) - \mathcal{G}(\mathbf{q}) + J_c(\mathbf{q})^T\mathbf{f}_c\Big)\\ 0 &= \mathbf{g_c}(\mathbf{q})\end{aligned}$$

where $\mathcal{M}$ is the square, positive-definite mass-inertia matrix, $\mathcal{C}$ contains the Coriolis and centrifugal forces, $\mathcal{G}$ the gravitational forces, and $\mathbf{u}(t)$ are the control input functions which are mapped with the constant matrix $\mathbf{S}$ to the actively controlled joints. The ground contact constraints $\mathbf{g_c}$ represent holonomic constraints on the system from which the constraint Jacobian may be obtained $J_c = \frac{\partial \mathbf{g_c}}{\partial \mathbf{q}}$, while $\mathbf{f}_c$ is the ground constraint force and k is a kinematic function relating $\dot{\mathbf{q}}$ and $\mathbf{v}$. These equations are evaluated using recursive, multibody algorithms as described in [13, 14].

The performance index to be minimized is the squared input torque u

$$\min_u \left\{ \int_0^{t_f} u^T u \, \mathrm{d}t \right\} \tag{1}$$

while the maximum power consumption M_W must satisfy the inequality constraint

$$\max_{t\in[0,t_f],\ i\in\{1,\ldots,n\}} |\dot{q}_i(t)\, u_i(t)| \le M_W, \tag{2}$$

where $\dot{\mathbf{q}}$ is the angular velocity and n is the total number of links.

Both biped models are optimized at two different average forward velocities: 0.417 m/s (1.5 km/h) and 0.555 m/s (2.0 km/h). This results in 4 different models which are optimized separately. The nomenclature of the four models is as follows: "Model 1" refers to the 12 kg robot moving at 0.417 m/s while "Model 2" has the same mass and walks at 0.555 m/s. The 18 kg version at 0.417 m/s is called "Model 3" and fast walking at 0.555 m/s is abbreviated by "Model 4." The resulting optimal control problems have been solved numerically using the method of direct collocation which is based on parameterization of state and control variables by piecewise polynomials and on sparse, large-scale sequential quadratic programming [13–15].

Commercial high performance motors are available with a wide range of power, torque, and speed output characteristics. A significant void in motor availability, however, generally exists between motors with a $20-25$W maximum power output and those with already a 70W max power output, the latter having a much increased weight. For this reason, both Models 1 & 2 were optimized with a maximum power output (2) of $M_W = 20$W in each joint. The optimization problem using Models 3 & 4 was not solvable for $M_W = 20$W, most likely due to the fact that the forward velocity constraints could not be met given the increased weight and limited power availability. Thus, M_W needed to be set higher for the heavier models, where M_W was set for Model 3 at $M_W = 25$W and Model 4 at $M_W = 40$W.

With each model the optimal control problem for one step has been solved numerically to obtain the solution trajectories of joint velocities and accelerations.

2.3 Summary of Different Models

Spikes in the torque and speed requirements depicted in Fig. 2 are a consequence of the model and moving at a high average forward velocity. These occur

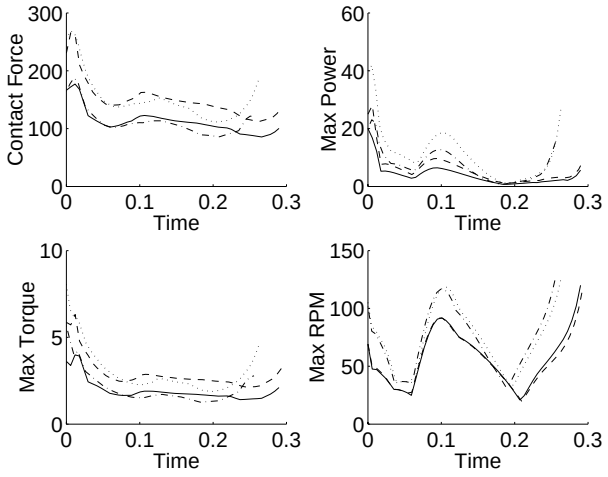

Figure 2: *Model 1: solid line, Model 2: dashdot, Model 3: dashed, Model 4: dotted*

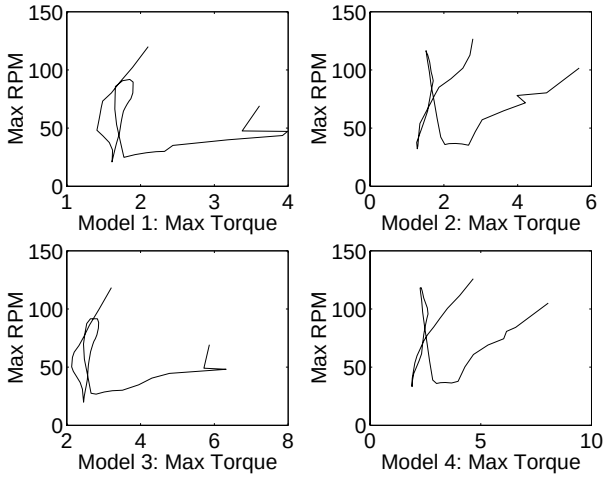

Figure 3: *Torque vs RPM from all 4 models.*

near the time of collision of the leg with the ground. It is believed that a well-designed foot construction including damping elements can avoid these peaks which are therefore neglected in the discussion of the motor characteristics. A foot will also allow the biped to make larger and fewer steps to travel the same distance, thus reducing the predicted high values for the joint velocities.

As the available maximum torque of a motor depends on its actual turning speed, it is interesting to see how these characteristics are connected as shown in Fig. 3. The task of drive selection is to find a drivetrain covering all these operation points. Taking these points into consideration and the previous data, the required motor characteristics are summarized in Table 2.

These data now are the basis for the selection of an appropriate motor-gear combination.

Table 2: *Motor characteristics for the 12 and 18 kg models.*

	12 kg model	18 kg model
Operational torque:	1.5–2.5 Nm	2.5–3.5 Nm
Maximum torque:	3.0 Nm	4.0 Nm
Operational RPM:	50–75 rpm	65–90 rpm
Maximum RPM:	90 rpm	100 rpm
Maximum Power:	15 W	20 W

2.4 Motor Selection

The calculated walking data is now used to select the voltage rating and gear ratio from a Maxon RE25, 20W motor and a Maxon GP32A gear. The Maxon motor was chosen because of the high torque to weight ratio.

Selecting a gear ratio basically means to find a suitable compromise between maximum RPM and maximum torque, i.e. to find a motor/gear combination such that the set of all points plotted in Fig. 3 is a subset of area reachable with that combination. Hence the reachable area now has to be determined.

The required motor torques T_m are calculated from the chosen gear ratio N_i and efficiency h_i

$$T_m = \frac{T}{N_i \, h_i}, \tag{3}$$

while the required motor speed $n_r = n_o \, N_i$ is the desired gear output speed n_o multiplied by the gear ratio N_i.

For each given gear ratio three different motor voltage ratings $V_m = \{30\text{V}, 42\text{V}, 48\text{V}\}$ are considered. The battery supply voltage of $V_s = 38\text{V}$ is assumed, delivered by three batteries providing 14.4 V each. The motor characteristic line is calculated by first determining the no-load motor speed n_{mV} from its rated value n_m and adjusted according to the supply voltage V_s

$$n_{mV} = n_m \frac{V_s}{V_m}. \tag{4}$$

The given slope of each motor characteristic line determines the reachable torque and velocity combinations as the set of all points below the line. The desired workspace of the motor thus should lie beneath this line.

A notable outcome of these calculations is the fact that the desired workspace for a 18 kg robot is not as well covered by the motor characteristic lines as with the 12 kg robot. Thus, the heavier robot will not be able to be driven nearly as fast as the lighter one; a traveling speed of 0.417 m/s still is achievable. The best choice appears to be a 42 V motor with a 66:1 gear ratio. The 30 V motor would probably have difficulties handling a 38 V battery supply.

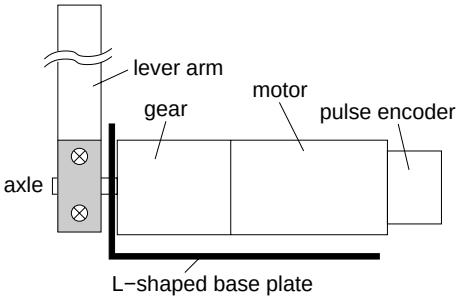

Figure 4: *Schematic of a joint.*

3 Mechanical Realization of the Biped

Based on the numerical results presented above, a 17 DoF robot – now including an additional navel joint – has been built. This section first discusses the hardware realization and the software environment used to control the robot. The achievable performance of a newly developed microcontroller based motion control board with USB connection is investigated in Sec. 3.2.

3.1 Hardware Design and Software Environment

For simplicity of design, one important aim was to assemble the robot from as many identical modules as possible. Therefore all joints are variations of the elementary joint shown in Fig. 4: The shaft of the motor-gear-unit is fixed to an L-shaped base plate. Attached to the axis of the motor is a lever arm whose far end is connected to the base plate of the next joint. Though this lightweight construction spares additional bearings the motor axis is still sufficiently stable to support the exerted load. For the links between the motors ordinary steel with a rectangular profile of $3 \times 15\,\mathrm{mm}^2$ is used. This slightly flexible construction was chosen to incorporate an additional mechanical shock absorption mechanism damping the impact of the feet hitting the ground. Joints requiring more than one DoF, like the ankle or the hip, are realized by two or more sequential motors with orthogonally oriented axes of rotation, see Fig. 6.

The mechanical robot construction arising from linking these elementary modules is shown in Figs. 5 and 6. The robot carries 3 batteries as power supply, two of them visible on the picture at the height of the hips and below the navel joint. The third battery is located symmetrically behind the hips together with an ATX power supply for the main PC which covers the upper body. The chosen Sony BP-L90A batteries provide a capacity of 90 Wh each, hence allowing for approximately 45 min autonomous walking.

The motors are accessed using the microcontroller

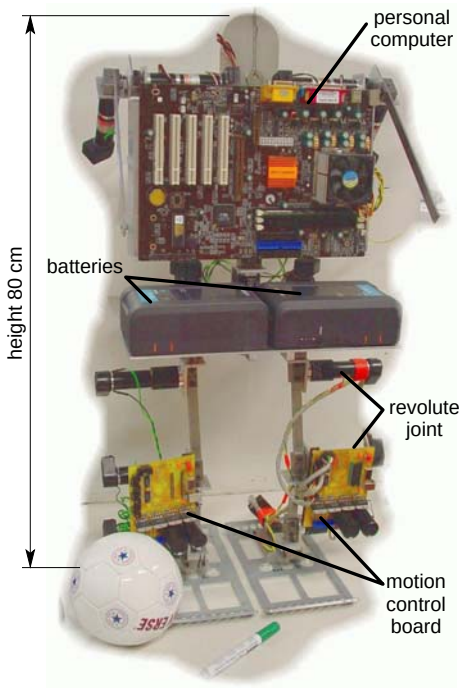

Figure 5: *Mechanical realization of the robot.*

board shown in Figs. 5 and 6 which was developed at the Control Systems Group in Berlin [16]. The core of the board is a Motorola MC68HC908BD48 8 bit microcontroller including: 3 USB endpoints, a 6 channel A/D converter and a 16 channel pulse-width modulator (PWM). These PWM signals are amplified by a National LMD18200 mosfet H-bridge, hence a motor load of up to 3 A at 55 V is admissible. The actual position of a motor is determined by evaluating the signals of pulse encoders attached to each motor using US Digital LS7266 quadrature decoders. To each board weighing 170 g, 4 motors can be connected. Hence this board represents a lightweight motion control solution.

With these components position PD control loops are implemented on the microcontroller. The A/D converters on the microcontroller are wired to sense the motor current which also allows to drive the motors with current control. These motion control boards are linked with the main PC on the robot via an USB connection. Through this link, new control inputs are delivered to the board retrieving the measured values at the same transfer stage.

For a main computer carried along by the robot a fullsize ATX mainboard is used. Being similar in weight compared to most full sized single board computers with equivalent computational power, a fullsize computer can be tolerated. The PC is equipped with an Athlon 1300 MHz CPU providing enough computational power for motion control and additional tasks such as object recognition using a camera system.

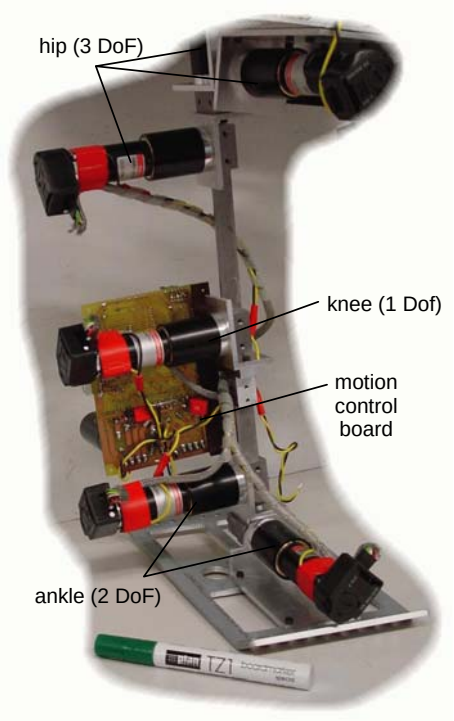

Figure 6: *Right leg rear view.*

To obtain a graphical interface to the robot and the motion control boards, a MATLAB S-function has been implemented allowing to drive the robot from within the SIMULINK simulation environment. Experiments showed, that this rapid prototyping environment handles well the soft realtime constraints for the outer control loop without the need for a hard realtime environment as presented in [17]. This may be attributable to the efficient task scheduling capabilities of the Linux kernel.

Based on this rapid control prototyping framework, future experiments can easily be implemented. The next section discusses the performance achievable with the decentralized solution using the microcontroller with USB connection to the PC.

3.2 Performance of the Motion Control Board

In a first step, the performance of the microcontroller is investigated. One important aspect is the maximally achievable sampling rate for the control loop.

In order to obtain a sufficient minimal angle resolution, a 16 bit representation is used to index a 360° workspace. Hence computation is time consuming on an 8 bit microcontroller. With the current implementation of a PD position control loop for four motors, the time required for reading the actual position of the motors from the external pulse decoders, computing and applying a new control signal is 1.8 ms. As the USB communication requires another 2 ms

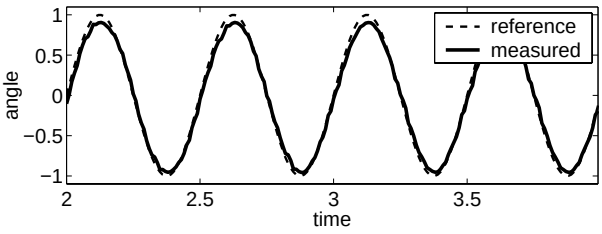

Figure 7: *Trajectory following with position control.*

computation time on the microcontroller, an overall sampling rate for the position control loop of 250 Hz is achieved. Although this sampling rate delivers satisfactory control results, first examinations foster the hope that this performance can be significantly increased by further code optimization by a more efficient C-compiler.

The reference signal which is provided through the USB bus also can be delivered at the same rate. The PC has to send a set of four reference signals to the board and recieves the latest four measured signals in return. Measurements of communication timing with two microcontroller boards attached have shown a mean communication time of 4.00 ms per board with a variance of $0.0084\,(\mathrm{ms})^2$. This low jitter can be attributed to the efficient task scheduling mechanism of the Linux kernel hence offering acceptable soft realtime capabilities on a machine with low system load. Implementing the data exchange with each board in separate threads, all boards can be provided with reference signals simultaneously, i.e. the communication times are not cummulative.

To test the trajectory tracking capabilities of the PD controller running at 250 Hz, a 292 g weight at the end of a 26.5 cm link has been attached to a motor. With this load the motor was commanded a 2 Hz sine reference trajectory, plotted as a dashed line in Fig. 7. One can see, that the measured position depicted as a solid line follows nicely the commanded trajectory.

Summarizing the results for the microcontroller board, a local control loop at 250 Hz can be implemented including the exchange of reference signal and measured values with a PC via USB. These rates are sufficient for motion control and prove the choice of USB for data exchange suitable for the desired purpose.

4 Conclusions and Outlook

In this paper the design of a new, autonomous walking robot with 17 DoF has been presented. The design is optimized for high speed walking with up to 3 steps per second, or equivalently about 0.5 m/s. Another constraint for the design was easy manufacturability, hence the robot is composed of as many

identical mechatronic modules as possible. Detailed numerical simulation and optimization of motion dynamics is used in each step of the design and control development process.

The hardware realization of the afore discussed biped robot has been described in detail including a newly developed USB motion control board. First experiments validating this motion control board show accurate trajectory tracking capabilities proving the concept of a microcontroller communicating with a PC through USB suitable for control applications. This is regarded as crucial for the success of the biped walking project, as the motion control board solution represents a lightweight interface between the PC and the robot hardware. Due to this microcontroller solution a dedicated realtime environment on the PC proved not to be necessary. Performance of the motors so far are in line with theoretical considerations on the choice of a motor-gear-combination.

The next goal will be to make the robot walk. This incorporates the solution of many detail problems and improvements: a three-dimensional mathematical model with swinging arms for improved stability and walking speed has to be developed as well as several sensors such as foot contract sensors and gyroscopes have to be mechanically and electronically integrated.

Acknowledgments — Technical support by U. Weidauer and S. Schostan is appreciated. The motion control board has been mainly developed by K. Gänger, see [16].

References

[1] Y. Fujimoto and A. Kawamura, "Simulation of an Autonomous Biped Walking Robot Including Environmental Force Interaction," *IEEE Robotics and Automation Magazine*, vol. 5(2), pp. 33–42, June 1998.

[2] M. Inaba, T. Igarashi, S. Kagami, and H. Inoue, "A 35 DOF Humanoid that can Coordinate Arms and Legs in Standing up, Reaching and Grasping an Object," in *Proceedings of the IEEE/RSJ International Conference on Intelligent Robots and Systems IROS*, (Osaka, Japan), pp. 29–36, 1996.

[3] J. Laci, H. Hooshang, and C. Bradley, "A Control Strategy for Adaptive Bipedal Locomotion," in *Proceedings of the IEEE International Conference on Robotics and Automation*, (Minneapolis, Minnesota), pp. 563–569, 1996.

[4] K. Hirai, "Current and Future Perspective of Honda Humanoid Robot," in *Proceedings of the IEEE/RSJ International Conference on Intelligent Robots and Systems IROS*, (Grenoble, France), pp. 500–508, 1997.

[5] K. Hirai, M. Hirose, Y. Haikawa, and T. Takenaka, "The Development of Honda Humanoid Robot," in *Proceedings of the IEEE International Conference on Robotics and Automation*, (Leuven, Belgium), pp. 1321–1326, 1998.

[6] M. Hirose, Y. Haikawa, T. Takenaka, and K. Hirai, "Development of Humanoid Robot ASIMO," in *IEEE/RSJ International Conference on Intelligent Robots and Systems (IROS) – Workshop 2*, (Maui, Hawaii), 2001.

[7] Y. Kuroki, T. Ishida, and J. Yamaguchi, "A Small Biped Entertainment Robot SDR-3X," in *IEEE/RSJ International Conference on Intelligent Robots and Systems (IROS) – Workshop 2*, (Maui, Hawaii), 2001.

[8] Y. Kuroki, T. Ishida, J. Yamaguchi, M. Fujita, and T. T. Doi, "A Small Biped Entertainment Robot," in *Proceedings of the International Conference on Humanoid Robots*, (Tokyo, Japan), pp. 181–186, 2001.

[9] M. Yamataka, H. Nakanishi, K. Yamabuchi, and A. Nakamura, "Development of a Small Animal-type Biped Robot and its Walking Control System," in *Proceedings of the International Conference on Humanoid Robots*, (Tokyo, Japan), pp. 197–204, 2001.

[10] H. Inoue and H. Hirukawa, "Explorations of Humanoid Robot Applications," in *Proceedings of the International Conference on Humanoid Robots*, (Tokyo, Japan), pp. 497–499, 2001.

[11] F. Yamasaki, T. Miyashita, T. Matsui, and H. Kitano, "PINO the Humanoid : A basic Architecture," in *Proceedings of the 4th International Workshop on RoboCup*, (Melbourne, Australia), 2000.

[12] The RoboCup Federation, *RoboCup Humanoid League 2002 Rule*. `http://www.robocup.org/-regulations/humanoid/rule_humanoid.htm`, 2002.

[13] M. Hardt and O. von Stryk, "The role of motion dynamics in the design, control and stability of bipedal and quadrupedal robots," in *Proc. RoboCup 2002 International Symposium*, (Fukuoka, Japan), 2002.

[14] M. Hardt and O. von Stryk, "Increasing stability in dynamic gaits using numerical optimization," in *Proc. 15th IFAC World Congress*, (Barcelona, Spain), 2002.

[15] O. von Stryk, *User's Guide for DIRCOL Version 2.1*. Simulation and Systems Optimization Group, Technische Universität Darmstadt, `www.sim.informatik.tu-darmstadt.de/sw/dircol/`.

[16] K. Gänger, "Implementieren einer Regelungselektronik fuer Humanoide Fussball-Roboter (*in German*)," tech. rep., Control Systems Group Berlin, 2002.

[17] D. Wollherr and M. Buss, "Cost Oriented VR-Simulation Environment for Computer Aided Control Design," in *Proceedings of the 6th IFAC Symposium on Cost Oriented Automation*, (Berlin, Germany), 2001.